INORGANIC CHEMISTRY FRONTIERS

RESEARCH ARTICLE

View Article Online
View Journal | View Issue

Cite this: *Inorg. Chem. Front.*, 2022, **9**, 3566

W^{VI}–OH functionality on polyoxometalates for water reduction to molecular hydrogen†

Sateesh Mulkapuri, Athira Ravi, Subhabrata Mukhopadhyay, Sathish Kumar Kurapati, Vinaya Siby and Samar K. Das *

Received 23rd February 2022,
Accepted 26th May 2022

DOI: 10.1039/d2qi00421f

rsc.li/frontiers-inorganic

Grafting a W^{VI}–$(OH)_2$ functionality on the surface of polyoxometalates (POMs) makes the concerned POM compounds, $Na_6[\{Co^{II}(H_2O)_3\}_2\{W^{VI}(OH)_2\}_2\{(Bi^{III}W^{VI}_9O_{33})_2\}]\cdot 8H_2O$ (**1**) and $Na_4(Himi)_2[\{Mn^{II}(H_2O)_3\}_2\{W^{VI}(OH)_2\}_2\{(Bi^{III}W^{VI}_9O_{33})_2\}]\cdot 28H_2O$ (**2**) prominent heterogeneous electrocatalysts for water reduction to molecular hydrogen. We have identified that the W^{VI}–$(OH)_2$ functionality acts as the active site for electrocatalytic hydrogen evolution reaction (HER). The chances of *in situ* generation and participation of secondary species (metal nanoparticles *etc.*) in the present electrocatalysis have been eliminated by performing controlled experiments. The electrocatalysts **1** and **2** are stable enough towards HER up to 1000 cycles of cyclic voltammetric measurement and 10 hours chronoamperometry. The relevant turnover frequencies of **1** and **2** are 0.593 s^{-1} and 0.634 s^{-1} respectively exhibiting high efficiency towards electrocatalytic HER. This work has potential to generalize that POMs having M–OH functionality attached on its cluster surface would function as catalysts for HER.

Introduction

Scientists, worldwide, have realized that hydrogen energy can be considered as the next-generation energy source, because this carbon-free energy source possesses desired high energy density (146 kJ g^{-1}).[1–7] The electrochemical water splitting can produce H_2 in a sustainable manner.[7] The overall electrochemical water splitting consists of the oxygen evolution reaction (OER) and hydrogen evolution reaction (HER).[1–10]

In acidic pH, the water oxidation to molecular oxygen (eqn (1)) and proton reduction to molecular hydrogen (eqn (2)) form the overall water splitting reactions (eqn (1) and (2)). In neutral and basic pH, the half-reactions are described by eqn (3) and (4). The shift in the half-cell reactions is governed by the change in pH *i.e.*, by the change in the relative concentrations of H^+ and OH^- in water.

Acidic medium

Anode:

$$2H^+ + O_2 + 4e^- \rightleftharpoons 2H_2O \quad E^\circ = +1.23\ V \qquad (1)$$

Cathode:

$$2H^+ + 2e^- \rightleftharpoons H_2 \quad E^\circ = 0.00\ V \qquad (2)$$

Alkaline medium

Anode:

$$O_2 + 2H_2O + 4e^- \rightleftharpoons 4OH^- \quad E^\circ = +0.40\ V \qquad (3)$$

Cathode:

$$4H_2O + 4e^- \rightleftharpoons 2H_2 + 4OH^- \quad E^\circ = -0.83\ V \qquad (4)$$

Significant advances have been made in the development of noble metal-free electrocatalysts for HER (eqn (2) and (4)) in the last few decades. Zou *et al.*, have reviewed several noble-metal-free metal electrocatalysts, which work in a heterogeneous manner, *e.g.*, metal sulphides, metal selenides, metal carbides, metal nitrides, metal phosphides, heteroatom-doped nanocarbons, *etc.*[7] The reported catalytic studies on HER are mainly performed in acidic conditions.[6–8,11–14] In an acidic medium, HER is thermodynamically feasible. Moreover, it also follows a simple reaction pathway: $2H^+ + 2e^- \rightleftharpoons H_2$, for which the mechanism [the Volmer step, $H^+ + e^- \rightarrow H_{ads}$ (adsorbed hydrogen atom on the electrode surface), followed by the Tafel step ($2H_{ads} \rightarrow H_2$) or the Heyrovsky step ($H_{ads} + H^+ + e^- \rightarrow H_2$) or both together resulting in HER], is well established. In this direction, polyoxometalate (POM) based catalysts can be the best choice for water splitting, because POMs not only show huge applications in diverse areas including medicinal

School of Chemistry, University of Hyderabad, P.O. Central University, Hyderabad – 500046, India. E-mail: skdas@uohyd.ac.in; Fax: +91-40-2301-2460; Tel: +91-40-2313-4853

†Electronic supplementary information (ESI) available: Details of physical characterizations such as tables and figures for SC-XRD and CSD 2033177 and BVS, XPS, PXRD, electrode preparation, electrochemical measurements, and analyses, GC, FESEM-EDX, *etc.* CCDC 2033177. For ESI and crystallographic data in CIF or other electronic format see DOI: https://doi.org/10.1039/d2qi00421f

science,[15] magnetism,[16,17] photo-/electro-chemical water splitting,[7,18–25] *etc.* but also are earth-abundant metal-oxides (inexpensive materials) and most of them can hold a large number of electrons reversibly,[26,27] exhibiting rich redox chemistry while maintaining the structural integrity in an acidic aqueous solution.[28–30]

We have synthesized and structurally characterized a sandwich-type POM-based compound where a $[\{Co^{II}(H_2O)_3\}_2\{W^{VI}(OH)_2\}_2]^{12+}$ core is sandwiched by two $\{Bi^{III}W_9^{VI}O_{33}\}^{9-}$ units. The compound is formulated as $Na_6[\{Co^{II}(H_2O)_3\}_2\{W^{VI}(OH)_2\}_2\{(Bi^{III}W_9^{VI}O_{33})_2\}]\cdot 8H_2O$ (**1**), having two *cis*-$\{W^{VI}(OH)_2\}$ functional units for electrocatalytic hydrogen evolution reaction (HER) by water reduction.

Apart from the classic Krebs compound $Na_{12}[(W^{VI}O_2(OH))_2(W^{VI}O_2)_2(Bi^{III}W_9^{VI}O_{33})_2]\cdot 44H_2O$ (also formulated as $Na_{12}[Bi_2W_{22}O_{74}(OH)_2]\cdot 44H_2O$)[31] and $Na_4(H_2imi)_2[\{Zn^{II}(H_2O)_3\}_2\{W^{VI}O(OH)\}_2\{(Bi^{III}W_9^{VI}O_{33})_2\}]\cdot 25H_2O$[32] having two W–OH moieties, two more POM based compounds containing the *cis*-$\{W^{VI}(OH)_2\}$ units namely, $Na_4(Himi)_2[\{Mn^{II}(H_2O)_3\}_2\{W^{VI}(OH)_2\}_2\{(Bi^{III}W_9^{VI}O_{33})_2\}]\cdot 28H_2O$ (**2**)[33] and $Na_4(Himi)_2[\{Co^{II}(H_2O)_3\}_2\{W^{VI}(OH)_2\}_2\{(Bi^{III}W_9^{VI}O_{33})_2\}]\cdot 31H_2O$ (**BWCN**),[34] have been reported by Zhou–Liu–Yang groups and Zhou–Liu groups, respectively. Both the compounds, **2** and **BWCN** can perform HER in acidic pH 4. A detailed account of electrocatalytic HER by water reduction at a mildly acidic pH 4, catalyzed by compounds **1** and **2**, has been described here. Since the cluster (anionic) part of **BWCN** and compound **1** are essentially identical, we have not explored further the electrocatalytic properties of **BWCN**. This report establishes a new insight in POM chemistry that a $\{W^{VI}$–OH$\}$ functionality on a POM cluster surface can function as an active site for HER.

Experimental

Materials and methods

All the experiments were conducted with deionized water under ambient atmospheric conditions and chemicals were used as received of analytical reagent grade without further purification.

Synthesis of polyoxometalates (POMs). Compound $Na_6[\{Co^{II}(H_2O)_3\}_2\{W^{VI}(OH)_2\}_2\{(Bi^{III}W_9^{VI}O_{33})_2\}]\cdot 8H_2O$ (**1**) was isolated in a one-pot wet synthesis (see below), whereas the compound $Na_4(Himi)_2[\{Mn^{II}(H_2O)_3\}_2\{W^{VI}(OH)_2\}_2\{(Bi^{III}W_9^{VI}O_{33})_2\}]\cdot 28H_2O$ (**2**) was prepared according to the literature procedure.[33]

Synthesis of $Na_6[\{Co^{II}(H_2O)_3\}_2\{W^{VI}(OH)_2\}_2\{(Bi^{III}W_9^{VI}O_{33})_2\}]\cdot 8H_2O$ (1). 0.5 mL of 6 M nitric acid (HNO_3) was added dropwise to the aqueous solution of sodium tungstate (9 mmol of $Na_2WO_4\cdot 2H_2O$ present in 25 mL of water) and heated at 90 °C for 15 min under stirring. The reaction mixture was removed from the hot plate and cooled to room temperature, and then filtered off to remove the traces of insoluble material. The cobalt nitrate solution (2 mmol of $Co(NO_3)_2\cdot 6H_2O$ dissolved in 2 mL of water) was added dropwise to the above colorless filtrate at room temperature under constant stirring, which turned to a purple color reaction mixture. Subsequently, a bismuth nitrate solution (1 mmol of $Bi(NO_3)_3\cdot 5H_2O$ in 1 mL of 6 M nitric acid) was added dropwise with vigorous stirring and the pH of the reaction mixture was adjusted to 6.82 using 15% aqueous ammonia solution. The reaction mixture was covered with a watch glass and again heated at 90 °C for 1 hour with continuous stirring. A blue-colored solution with a purple color slurry was formed and the reaction mixture was filtered hot. The purple-colored precipitate, that was formed again in the filtrate, after 4 hours, was removed by filtration. The clear filtrate was left for crystallization at room temperature. The block-type pink color crystals were obtained within ten days. The crystals were isolated by washing twice with a minimal amount of ice-cold water and kept for drying at room temperature. Yield: 1.65 g (61.84% based on tungsten). Elemental analysis: (%) calc. Bi: 7.12, Co: 2.01, Na: 2.35, W: 62.63 and (%) Found. Bi: 7.25, Co: 1.96, Na: 2.17, W: 62.89. FT-IR (4000–400 cm^{-1}): 3730, 3314, 1625, 941, 874, 831, 782, 730, 640, 579, 475.

Physical characterization. Single-crystal X-ray diffraction data were collected on Bruker D8 Quest CCD diffractometer with Mo-Kα (λ = 0.71073 Å) source (for details, see ESI section S1.1†). Powder X-ray diffraction (PXRD) data were recorded on Bruker D8-Advance diffractometer using graphite monochromated Cu Kα1 (1.5406 Å) and Kα2 (1.54439 Å) radiation. Elemental analyses were performed on ICP-OES Varian 720ES. Bruker Tensor II equipped with platinum attenuated total reflectance (ATR) accessory was used to collect IR spectra. Raman spectra were obtained with a Wi-Tec alpha 300 AR laser confocal optical microscope (T-LCM) facility equipped with a Peltier cooled CCD detector using 633 nm Argon ion laser. Electronic absorption spectra were obtained on the UV-2600 Shimadzu UV–visible spectrophotometer at room temperature. Field-emission scanning electron microscopy energy dispersive X-ray (FESEM-EDX) analysis was carried out with a Carl Zeiss model Ultra 55 microscope equipped with Oxford Instruments X-MaxN SDD (50 mm^2) system functioned with INCA software. X-ray photoelectron spectroscopy profiles were obtained with the Thermo Scientific K-ALPHA surface analysis spectrometer using Al Kα radiation (1486.6 eV). All the electrochemical studies performed on Zahner Zanium electrochemical workstation were operated with Thales software. GC experiments for the detection of electrochemically generated hydrogen gas were performed using Shimadzu Nexis GC-2030 equipment.

Electrochemical methods. The cyclic and linear sweep voltammograms were recorded at acidic pH 4.0 solution (0.1 M potassium phosphate electrolyte), under nitrogen atmosphere in heterogeneous mode using a conventional three-electrode setup. Compounds $Na_6[\{Co^{II}(H_2O)_3\}_2\{W^{VI}(OH)_2\}_2\{(Bi^{III}W_9^{VI}O_{33})_2\}]\cdot 8H_2O$ (**1**) and $Na_4(Himi)_2[\{Mn^{II}(H_2O)_3\}_2\{W^{VI}(OH)_2\}_2\{(Bi^{III}W_9^{VI}O_{33})_2\}]\cdot 28H_2O$ (**2**) modified nickel foam (NiFO) electrodes were used as working electrodes, while Ag/AgCl (3 M) and Pt-mesh electrodes were employed as reference and counter electrodes, respectively. All measurements were performed using 100 mV s^{-1} scan rate unless mentioned otherwise. The homogeneous cyclic and linear sweep voltammograms of water soluble compound $Na_{12}[(WO_2(OH))_2(WO_2)_2(BiW_9O_{33})_2]\cdot 44H_2O$ (hereafter named as compound **3**) were recorded using 1 mmol

compound in 0.1 M potassium phosphate electrolyte solution (pH 4.0). The concerned homogeneous CV and LSV profiles were collected with 3 mm glassy carbon electrode as working electrode, Ag/AgCl (3 M) as reference electrode and Pt-mesh as counter electrode in a similar experimental condition. All potentials were reported in terms of RHE, where $E_{(RHE)} = E_{(Ag/AgCl)} + 0.204\ V + 0.059pH$. The detailed relevant procedures can be found in section S2, ESI.†

Results and discussion

Synthesis

The cobalt incorporated anti-Lipscomb (Krebs type) compound $Na_6[\{Co^{II}(H_2O)_3\}_2\{W^{VI}(OH)_2\}_2\{(Bi^{III}W_9^{VI}O_{33})_2\}]\cdot 8H_2O$ (**1**) was obtained in a one-pot aqueous wet synthesis involving sodium tungstate, cobalt nitrate and bismuth nitrate. The molecular formula of compound **1** was derived from the single-crystal X-ray structure and elemental analyses including ICP-OES analysis. The synthesis of compound $Na_4(Himi)_2[\{Mn^{II}(H_2O)_3\}_2\{W^{VI}(OH)_2\}_2\{(Bi^{III}W_9^{VI}O_{33})_2\}]\cdot 28H_2O$ (**2**) was adapted from a reported procedure.[33] Compounds **1** and **2** have a common anionic component $[\{M^{II}(H_2O)_3\}_2\{W^{VI}(OH)_2\}_2\{(Bi^{III}W_9^{VI}O_{33})_2\}]^{6-}$ (M^{II} = Co and Mn) except the fact that M^{II} = Co(II) in **1** and Mn (II) in **2**. In the common cluster anion of the present study (compounds **1** and **2**), two identical tri-lacunary bowls, $\{BiW_9O_{33}\}^{9-}$ are joined together by two units of $\{W^{VI}(OH)_2\}^{4+}$ moieties resulting in a hypothetical entity of bis-dodecatungstate, $[\{W(OH)_2\}_2(BiW_9O_{33})_2]^{10-}$. This is further coordinated to two units of $\{M^{II}(H_2O)_3\}^{2+}$ (M = Co, Mn) to result in M^{II}-incorporated common heteropoly cluster anion $[\{M^{II}(H_2O)_3\}_2\{W(OH)_2\}_2(BiW_9O_{33})_2]^{6-}$ (M = Co, Mn) of compounds **1** and **2**. There are a number of POM compounds, that have bridging hydroxyl (OH^-) groups;[35–39] but there are only a few POM compounds having terminal M–OH, as found in the compounds $Na_{12}[(WO_2(OH))_2(WO_2)_2(BiW_9O_{33})_2]\cdot 44H_2O$ (**3**)[31] and $Na_4(H_2imi)_2[\{Zn^{II}(H_2O)_3\}_2\{W^{VI}O(OH)\}_2\{(Bi^{III}W_9^{VI}O_{33})_2\}]\cdot 25H_2O$.[32] And there are only two reported structurally characterized POM compounds, namely $Na_4(Himi)_2[\{Mn^{II}(H_2O)_3\}_2\{W^{VI}(OH)_2\}_2\{(Bi^{III}W_9^{VI}O_{33})_2\}]\cdot 28H_2O$ (**2**)[33] and $Na_4(Himi)_2[\{Co^{II}(H_2O)_3\}_2\{W^{VI}(OH)_2\}_2\{(Bi^{III}W_9^{VI}O_{33})_2\}]\cdot 31H_2O$ (**BWCN**),[34] to our knowledge, each of that have two terminal hydroxyl (OH) groups, *i.e.*, two *–cis*$\{W^{VI}(OH)_2\}^{4+}$ moieties.

Compound $Na_6[\{Co^{II}(H_2O)_3\}_2\{W^{VI}(OH)_2\}_2\{(Bi^{III}W_9^{VI}O_{33})_2\}]\cdot 8H_2O$ (**1**) in the present work is the third example of structurally characterized POM compound that has *–cis*$\{W^{VI}(OH)_2\}^{4+}$ functionality. This article has been coined to establish the importance of having *–cis*$\{W^{VI}(OH)_2\}^{4+}$ moiety on the POM cluster surface, which can act as the functional site for electrocatalytic water reduction to molecular hydrogen.

Crystal structure

Single-crystal X-ray diffraction (SCXRD) analysis reveals that compound **1** crystallizes in a monoclinic *C*2/*m* space group, while compound **2** crystallized in a triclinic *P*$\bar{1}$ space group.[33] The presence of protonated imidazole molecule in the crystal structure of **2**, probably, resulted in this difference. The six negative charges of the common heteropoly tungstate anion, $[\{M^{II}(H_2O)_3\}_2\{W(OH)_2\}_2(BiW_9O_{33})_2]^{6-}$, is counter-balanced by six Na^+ ions in compound **1** and by four Na^+ and two imidazolium $(Himi)^+$ cations in compound **2**.

The molecular structure of the cobalt-containing cluster anion $[\{Co(H_2O)_3\}_2\{W(OH)_2\}_2(BiW_9O_{33})_2]^{6-}$ in the crystal structure of compound **1** is shown in Fig. 1a. The Bi–O and O–W bond distances in Bi–O–W and W–O–W fragments within this POM cluster unit fall in the range of 2.1 to 2.2 Å, which are consistent with reported analogs.[25,31–35,40] The complete details of bond distances and bond angles are given in the crystallographic tables (see ESI, Fig. S1, Tables S1 and S2†). Notably, two units of the tungsten *–cis*$\{W^{VI}(OH)_2\}$ centres, present at the sandwiched positions, are geometrically/environmentally different from the other framework tungsten centers as shown in Fig. 1(b and c). In each of the $\{W^{VI}(OH)_2\}$ moieties, the W^{VI}

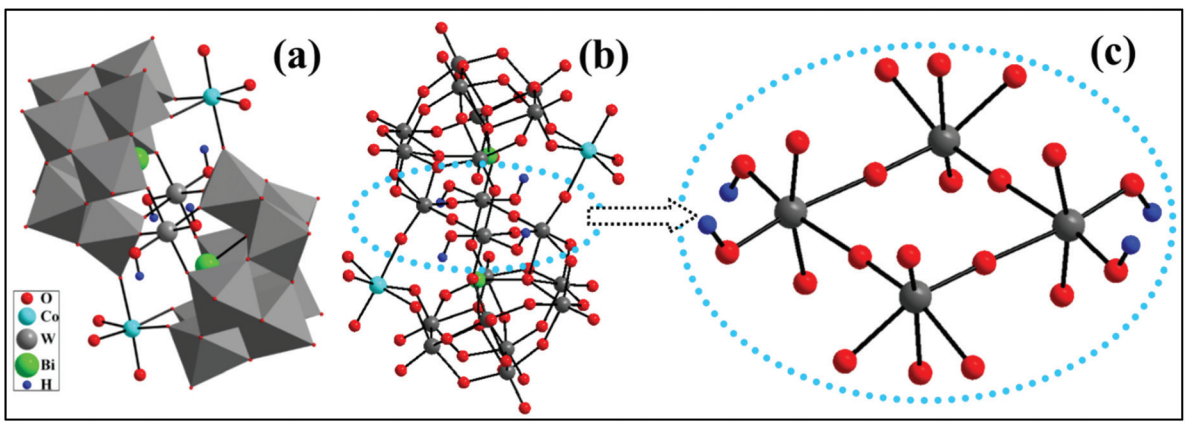

Fig. 1 (a and b) polyhedral and ball-stick representation of molecular structure of the compound **1**, (c) magnified view of *–cis*$\{W^{VI}(OH)_2\}$ core of compound **1** (W, grey; O, red; Co, cyan; H, blue).

center is coordinated by two hydroxyl groups that are *cis* to each other and symmetrically related. Thus, there are four W^{VI}–OH groups with identical W–OH bond distances of 1.839 Å. The bond valence sum (BVS) values of the hydroxyl oxygen (–OH) atoms in compounds **1**, **2**, and **BWCN**, respectively are 1.29, 1.30, 1.26 (see ESI, section S1.2†). This supports the presence of W–OH groups in compounds **1**, **2**, and **BWCN**.

FESEM-EDX and spectroscopy

In order to understand the surface elemental composition, the field emission scanning electron microscopy energy dispersive X-ray (FESEM-EDX) analyses have been carried out on both compounds **1** and **2** and we found the presence of their constituent elements (Fig. 2a and b). Further, X-ray photoelectron spectroscopy survey scans of compounds **1** and **2** have also confirmed the same (Fig. 2c). The XPS analyses of compounds **1** and **2** have been carried out with respect to the C1s peak at 284.8 eV.[41] In the XPS survey scan, the bands at 35.9, 159, 530, and 1072.5 eV for W 4f, Bi 4f, O 1s, and Na 1s respectively in compounds **1** and **2** have confirmed the presence of W, Bi, O, and Na. The bands at 779.3, and 641.6 eV for Co 2p and Mn 2p respectively have supported the existence of Co and Mn in compounds **1** and **2** (Fig. 2c). In the high-resolution X-ray photoelectron spectroscopy (HR-XPS) scan, the deconvoluted O 1s peaks at 530.22, and 530.24 in compound **1** and **2** respectively correspond to the existence of oxygen in the form of M–O–M (O^{2-}), whereas 532.51, and 531.69 eV in compounds **1** and **2** authenticates the existence of M–OH (–OH), (Fig. 2d and e). More precisely, the O 1s HR-XPS shoulder peak at 532.51 and 531.69 eV in compounds **1** and **2** respectively have strengthened the presence of metal-hydroxyl groups, *i.e.*, W–OH functionality.[42] The W 4f and Bi 4f HR-XPS peaks in both the compounds have shown that the tungsten and bismuth are present in 6+ and 3+ oxidation states respectively (see ESI, Fig. S4†). On the same line, the Co 2p and Mn 2p XPS bands in compounds **1** and **2** respectively have inferred that these metals are in their 2+ oxidation state (see ESI, Fig. S4†).

The FT-IR spectra of compounds **1** and **2**, as expected, have shown POM characteristic IR peaks in the region of 950 to 450 cm^{-1} for W=O, W–O–W, and Bi–O–W stretching and bending vibrations (Fig. 3a). The broadband around 3300 cm^{-1} in both implies the O–H stretching of lattice water. However, in compound **2** two weak bands at 2995 and 2850 cm^{-1} have resembled the N–H, C–H vibrations of the imidazole, which are expectedly absent in the IR spectrum of compound **1**. In addition to the support of SCXRD, BVS, and XPS, the presence of $-W(OH)_2$ functionality in these two compounds can also be supported by the appearance of a weak feature at around 3730 cm^{-1} in the IR spectra of compounds **1** and **2** (Fig. 3a and b).[43,44] The Raman spectra of compounds **1** and **2** feature a strong peak in the region of 883–950 cm^{-1} for terminal W=O bonds (Fig. 3c). There is a considerable shift of the main Raman band towards the high-energy side for compound **2** as shown in Fig. 3c. This is probably due to the involvement of imidazolium cation in the hydrogen interactions with the polyxometalate in compound **2**. Fig. 3d shows the d–d transitions in the region of 800 to 540 nm for the compounds **1** and **2** in their electronic spectra confirming the incorporation of Co^{2+} and Mn^{2+} in the respective systems. For both the compounds, a broad feature in the high-energy region is attributed to the ligand to metal charge transfer (LMCT) transition. The experimental PXRD profiles of compounds **1** and **2** are

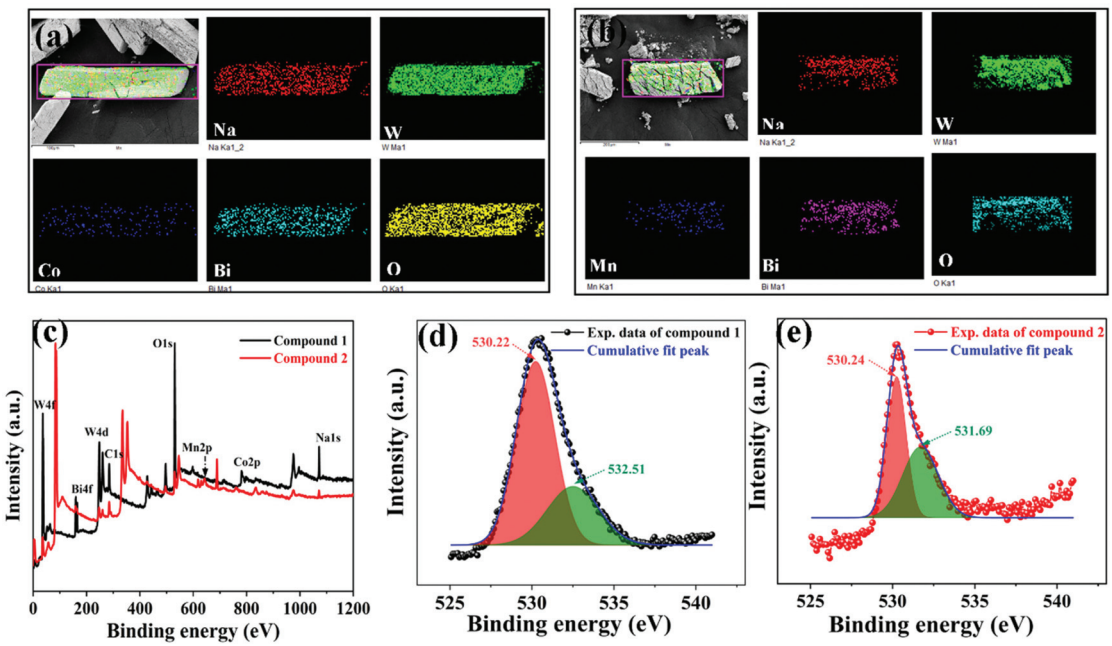

Fig. 2 (a and b) FESEM-EDX elemental mapping on compounds **1** and **2**, (c) X-ray photoelectron spectroscopy survey scan of compounds **1** and **2**, (d and e) O 1s core level X-ray photoelectron spectra of compounds **1** and **2**.

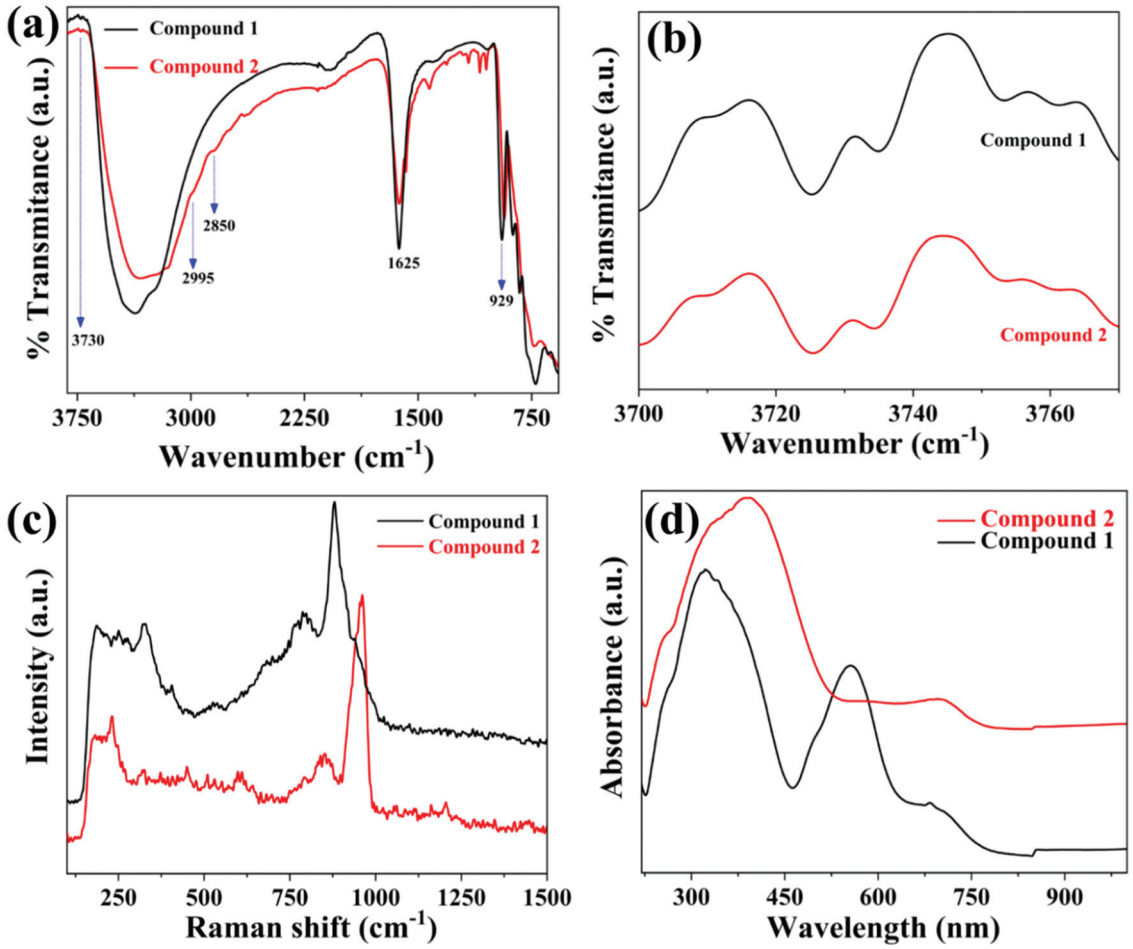

Fig. 3 (a) FT-IR spectra of the compounds **1** and **2**, (b) magnified view of W–OH FT-IR band in the region of 3700 to 3770 cm^{-1}, (c) Raman spectra of compounds **1** and **2**, (d) electronic spectra for compounds **1** and **2**.

found to be consistent with their respective simulated patterns (see ESI, Fig. S5†), which confirm the bulk purity and homogeneity of the synthesized materials (compounds **1** and **2**).

Electrocatalysis

Electrocatalytic hydrogen evolution reaction (HER). Hydrogen evolution reaction, catalyzed by compounds **1** and **2**, have been assessed by the cyclic and linear sweep voltammograms with the respective catalyst-modified nickel foam (NiFO) electrodes in an acidic pH 4.0 solution of 0.1 M potassium phosphate electrolyte. In Fig. 4a, the cyclic voltammograms of bare nickel foam (NiFO), compounds **1** and **2** have been displayed, where compounds **1** and **2** have shown a substantial catalytic current surge with the onset potentials at −0.360 and −0.285 V (*vs.* RHE) respectively corresponding to electrocatalytic HER; no comparable current was observed in the case of bare NiFO. Thus, in similar experimental conditions, compound **2** has exhibited an excellent HER activity over compound **1** in terms of the HER onset potential and current surge.

The hydrogen gas, generated electrocatalytically in our study, has been identified by the gas chromatograph (GC) experiments (see ESI, Fig. S6 and S7†). In order to further understand HER activity, the linear sweep voltammograms (LSVs) of compounds **1** and **2** were performed with a scan rate of 5 mV s^{-1} in an identical operational condition (Fig. 4b). As shown in Fig. 4b, the compounds **1** and **2** have demanded potentials of −0.693 and −0.652 V (*vs.* RHE) to attain the 10 mA cm^{-2} current density. The LSV curves of compounds **1** and **2** again infer that compound **2** has shown better activity than compound **1**. In the present work, in order to investigate the basis of HER, *i.e.*, whether it is water reduction (eqn (4)) or proton reduction (eqn (2)), we examined the CV features of catalyst-coated glassy carbon electrode in non-aqueous tetrahydrofuran (THF) containing 0.1 M tetrabutylammonium perchlorate (TBA-ClO_4) as supporting electrolyte with the sequential addition of a controlled amount of water which resulted in the chronological enhancement in cathodic catalytic current density for both **1**- and **2**- coated glassy carbon electrodes (see ESI, Fig. S8†). This suggests direct electrocatalytic water reduction (eqn (4)) catalyzed by compounds **1** and **2** under operational conditions.

W^{VI}–OH group on POM surface for HER by water reduction: validation of W^{VI}–OH functionality, accelerated durability

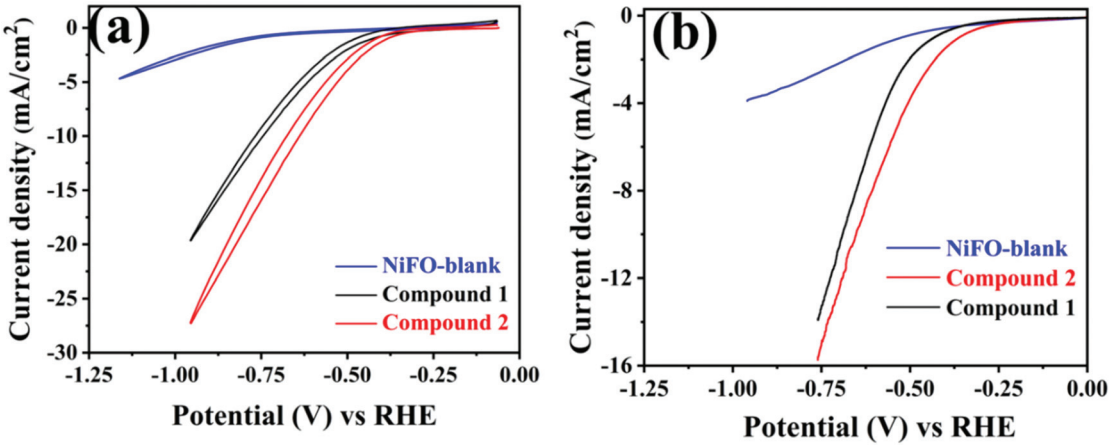

Fig. 4 (a) Cyclic voltammogram (CV) profiles of the NiFO-blank, compounds **1** and **2** recorded in a heterogeneous manner in 0.1 M potassium phosphate electrolyte (at acidic pH 4), (b) linear sweep voltammogram curves of the NiFO-blank and compounds **1** and **2** collected in 0.1 M potassium phosphate electrolyte (at acidic pH 4). All the CV scans were performed at a scan rate of 100 mV s^{-1} and LSVs were collected at a scan rate of 5 mV s^{-1}.

tests, and relevant controlled experiments. Transition metal-hydroxyl groups (*e.g.*, M^{n+}–OH) are chemically/electrochemically more reactive than the other forms of metal-oxo groups,[1,2,45] because metal-hydroxyl groups possess Brønsted acidity/more labile nature. There are reports on M^{n+}–OH functionality containing compounds exhibiting HER, but mostly without adequate emphasis on the structure–function relationship between the metal-hydroxyl group and HER.[46] For POM chemistry such accounts are rare.[47] The main theme of this article is to validate the role of W^{VI}–OH group on the electrochemical HER performed by compounds **1** and **2**, each having two symmetrical *cis*-$W^{VI}(OH)_2$ groups. As a part of controlled experiments, electrochemical analyses were performed on two more structurally relevant compounds, $Na_{12}[(WO_2(OH))_2(WO_2)_2(BiW_9O_{33})_2]\cdot 44H_2O$ (**3**) and $Na_{10}[Bi_2W_{20}Co_2O_{70}(H_2O)_6]\cdot 41H_2O$ (hereafter named as compound **4**), of which the former possess two W–OH groups and the later does not contain any W–OH group. Because of water-soluble nature of compound **3**, its cyclic and linear sweep voltammograms were performed homogeneously using 1 mmol compound **3** solution which was prepared in 0.1 M potassium phosphate electrolyte (pH 4.0). As evident from Fig. 5a–d, compounds **1–3** can perform electrocatalytic HER but no such catalytic current can be observed for compound **4** (which does not contain any M–OH functionality). This infers that: (i) the –W(OH) functionality containing POMs can perform electrocatalytic HER, (ii) there is no direct role of Co(II)-aqua/Mn(II)-aqua species on the electrocatalytic HER properties of compounds **1** and **2**, because the HER active compound **3** contains no such first-row transition metal ions but contains –W(OH) groups and (iii) structurally similar compound **4**, having –W═O groups and Co(II)-aqua species but not having –W(OH) groups, does not show electrocatalytic water reduction (Fig. 5c and d). These experiments strongly support that –$W^{VI}(OH)_2$ active sites of compounds **1** and **2** are responsible for electrocatalytic HER in the present study.

Long-term stability. In order to understand the long-term stability, accelerated durability tests of (i) 1000 cycles of cyclic voltammetry (from −0.05 V to −0.95 V *vs.* RHE) and (ii) chronoamperometry (CA) electrolysis at −0.81 V (*vs.* RHE) for 10 hours were performed using compounds **1**- and **2**-modified NiFO electrodes. As shown in Fig. 6a and b, no significant changes in HER curves and catalytic current have been occurred after 1000 cycles of cyclic voltammograms (CVs) for both the cases (compounds **1** and **2**), indicating that compounds **1** and **2** are stable enough during electrocatalytic HER for 1000 cycles of CVs. As shown in Fig. 6c, the derived plots of specific current density *versus* cycle number show no prominent drop in catalytic current in both cases even after 1000 cycles of CVs, retaining their HER current densities of −19.75 and −27.50 mA cm^{-2} for compounds **1** and **2**, respectively. Similarly, the chronoamperometry analyses for both the catalysts (**1** and **2**) show that both the compounds have notable long-term stability under operational conditions (at pH 4) exhibiting stable HER current densities of −10 and −12 mA cm^{-2} respectively at −0.81 V (*vs.* RHE) over the period of 10 hours as shown in Fig. 6d.

The structural integrity of the catalysts was thoroughly verified at the end of the accelerated HER durability tests by XPS, Raman spectral analyses, and FESEM-EDX analysis of the post-electrolysis electrode materials. The spectral features, recorded after electrolysis, are compared with those of the same materials (catalysts) recorded before electrochemical analysis.

The XPS (Fig. 7a and b) and Raman (see ESI, Fig. S9†) spectral features of the post-electrolyses electrode materials are consistent with those of electrode materials of compounds **1** and **2** before HER electrolyses. FESEM images of post-electrolysis electrode materials of compounds **1** and **2** are compared with those of before electrolysis materials in the section of ESI (see ESI, Fig. S10†). EDX elemental mappings (see ESI, Fig. S11–S14†) before and after HER electrolyses suggest no substantial changes in the elemental compositions of the elec-

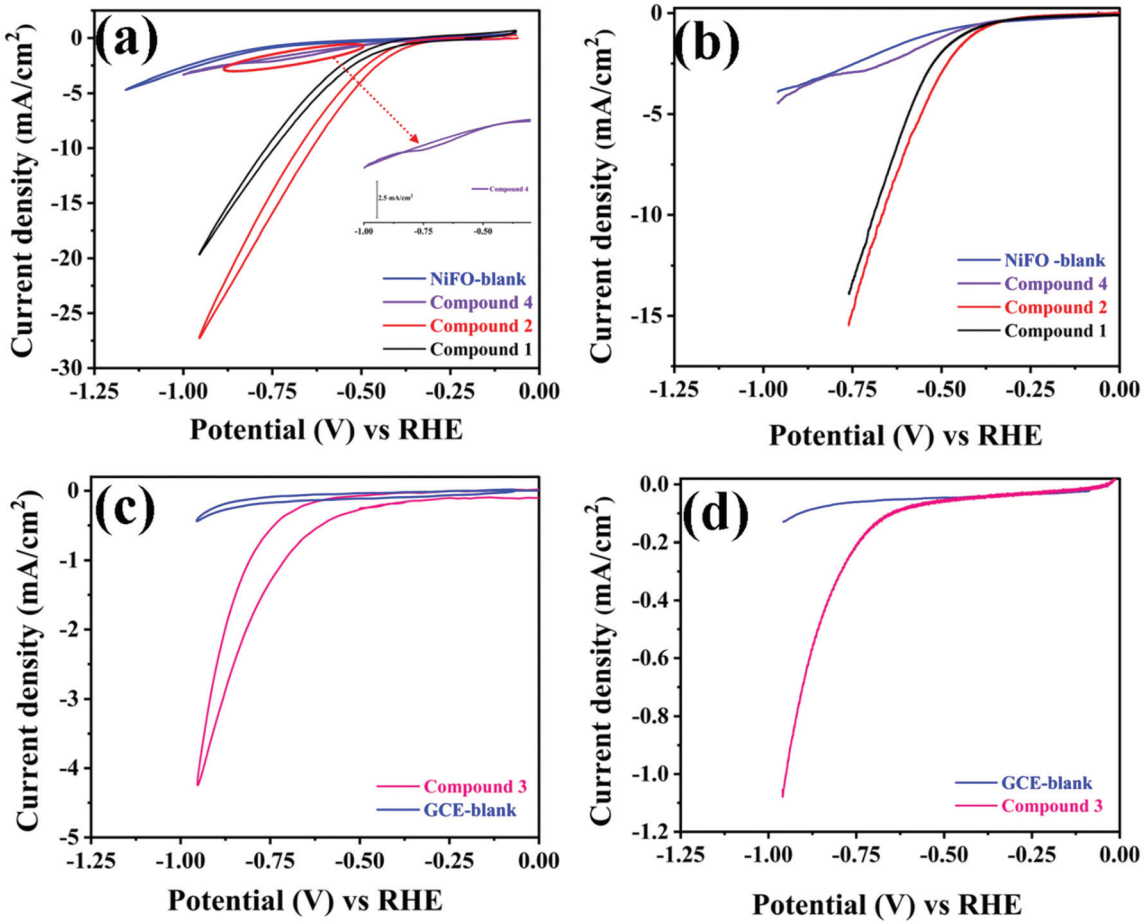

Fig. 5 (a) Cyclic voltammogram (CV) profiles of the NiFO-blank, compounds **1**, **2** and **4** recorded in a heterogeneous manner in 0.1 M potassium phosphate electrolyte (at acidic pH 4); inset, CV of compound **4** in an expanded form, (b) linear sweep voltammogram curves of the NiFO-blank and compounds **1**, **2** and **4** collected heterogeneously in 0.1 M potassium phosphate electrolyte (at acidic pH 4), (c and d) homogeneous CV and LSV profiles of glassy carbon electrode blank (GCE-blank) and compound **3** recorded using 1 mmol of compound **3** present in 0.1 M potassium phosphate electrolyte (at acidic pH 4). All the CV scans were performed at a scan rate of 100 mV s^{-1} and LSVs were collected at a scan rate of 5 mV s^{-1}.

trode materials of compounds **1** and **2** after electrolyses. All these experiments and the relevant results conclude that the POM-based compounds **1** and **2** function as true molecular catalysts for electrocatalytic HER in the mild-acidic condition of pH 4.0.

Kinetic insights. The Tafel plots have been constructed to investigate the kinetics of the electrocatalytic HER catalyzed by compounds **1** and **2** by carrying out galvanostatic polarization experiments under steady-state mass transfer. The observed Tafel slope values of 173.80 mV dec^{-1} and 152.07 mV dec^{-1} for compounds **1** and **2** respectively indicate that both the catalysts have efficient HER activity at acidic pH 4.0 (Fig. 8a). The hydrogen evolution reaction in the acidic medium, the mechanism of which is well-established, can be described by Volmer- and Heyrovsky-steps. It has been established that if the rate-determining step is water dissociation, *i.e.*, the Volmer step, as shown above, the theoretical value of the Tafel slope would be 118 mV dec^{-1}.[48] In the present electrocatalytic HER study, the values of experimentally observed Tafel slopes are in the range of 150–170 mV dec^{-1}, which is 30–50 mV dec^{-1} more than the theoretical value. This indicates the Volmer step as the rate-determining step in the present HER study. The increase in the Tafel slope value from the theoretically predicted value may be due to the slow combination of H_{ads} to form molecular hydrogen (H_2) in the Heyrovsky step or maybe the slow rate of mass transportation.[49] Further, to understand hydrogen evolution reaction electrode kinetics in terms of charge transfer resistance (R_{ct}), electrochemical impedance spectroscopy (EIS) for compounds **1** and **2** in the catalytic HER region has been performed (Fig. 8b) in the operational experimental conditions (at acidic pH 4.0), the relevant details have been given in the ESI (section S2.4†). The charge transfer resistance helps in understanding the electrochemical reaction kinetics at the electrode surface–electrolyte interface, where a lower R_{ct} value corresponds to the faster reaction kinetics. The obtained charge-transfer resistance (R_{ct}) values of 95.82 and 94.37 ohms for compounds **1** and **2** have followed the similar trend of Tafel slope values that the compound **2** is slightly better elec-

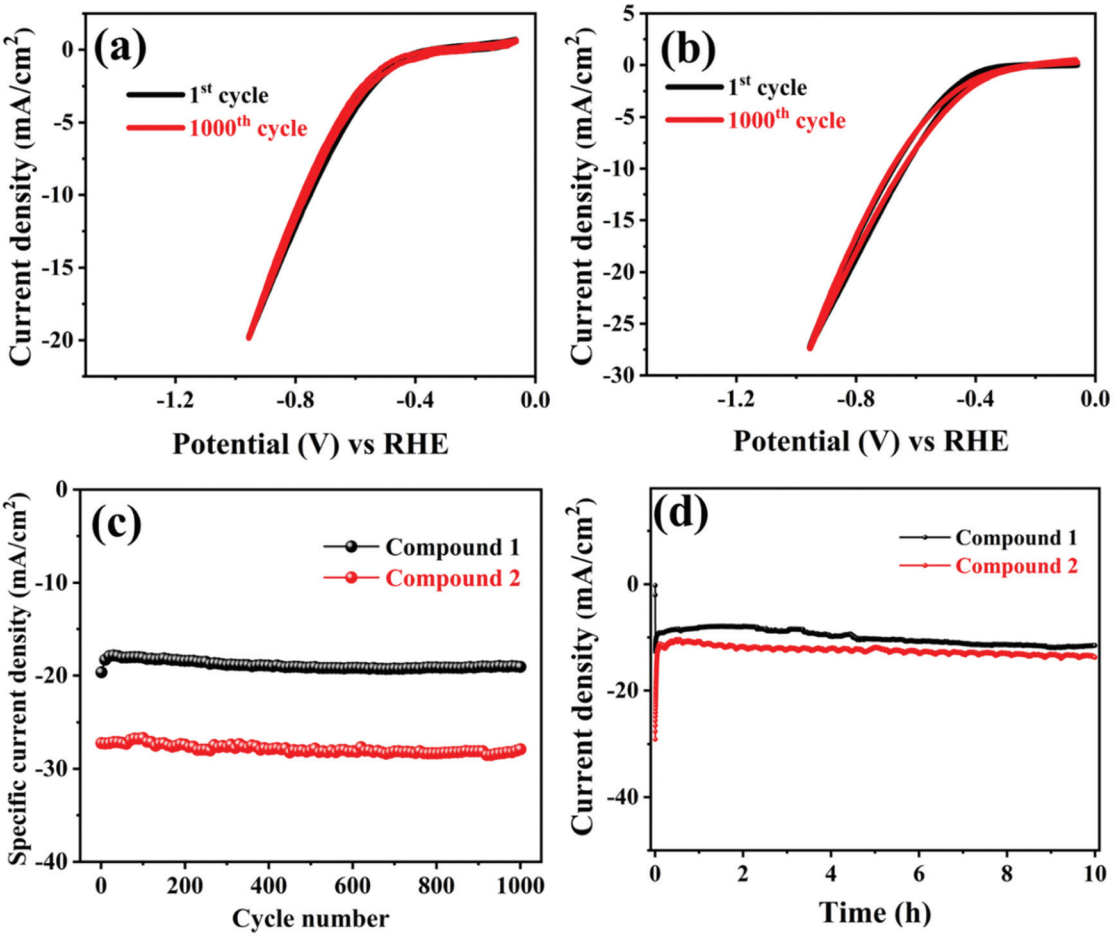

Fig. 6 (a and b) 1000 cycles of cyclic voltammogram profiles of the compounds **1** and **2** recorded in 0.1 M potassium phosphate electrolyte (at acidic pH 4), (c) derived plots of specific current density *vs.* the number of CV cycles for compounds **1** and **2** as heterogeneous catalysts (for every ten CV cycles one data point extracted), (d) chronoamperometry electrolysis responses of compounds **1** and **2** modified NiFO electrodes at −0.81 V (*vs.* RHE) for 10 hours collected in 0.1 M potassium phosphate electrolyte (at acidic pH 4). CVs were recorded with a scan rate of 100 mV s^{-1}.

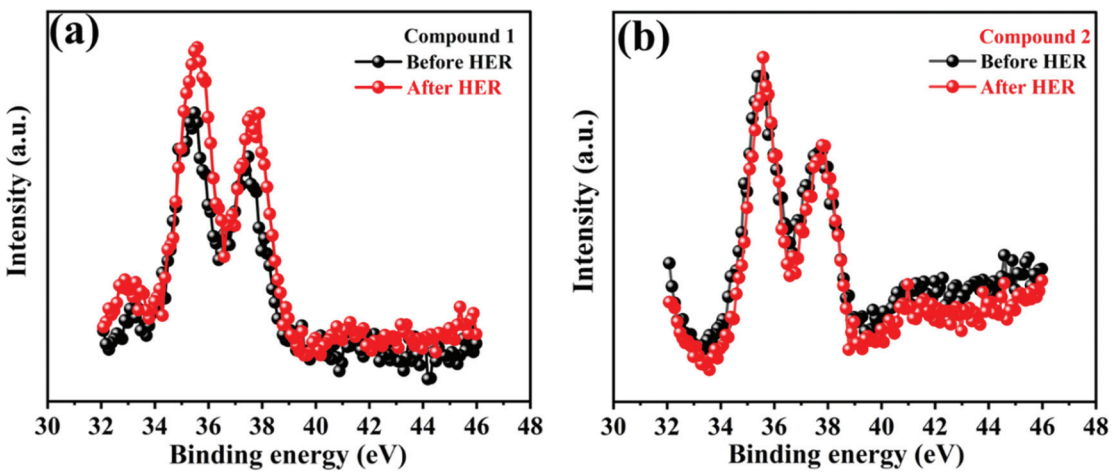

Fig. 7 Core level XPS spectral profiles of W 4f compared as before and after electrolysis for (a) compound **1** and (b) compound **2**.

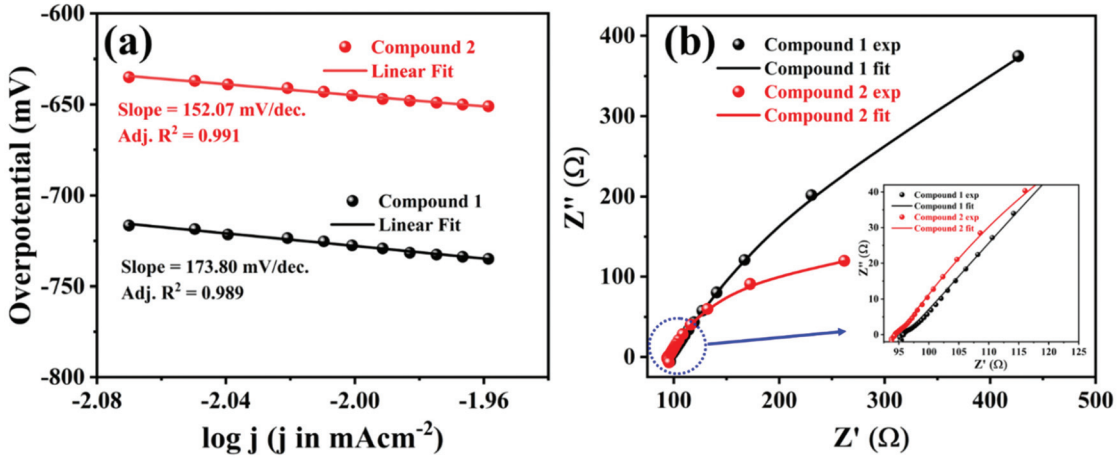

Fig. 8 (a) Tafel plots of compounds **1** and **2**, constructed in 0.1 M potassium phosphate electrolyte (at acidic pH 4.0) in a galvanostatic mode under study-state mass flow condition, (b) Nyquist plots of electrochemical impedance spectroscopy of compounds **1** and **2**, the inset of the Fig. 7b shows the magnified view of the Nyquist profiles of **1** and **2** in the region highlighted with a blue dotted circle.

trocatalyst for HER than compound **1** (lower the value of charge transfer resistance, more likely we get better catalytic performance). The double-layer capacitance (C_{dl}) value of a system is also helpful to understand the performance of an electrocatalyst. In order to obtain this value, we recorded cyclic voltammograms of both the catalyst-modified electrodes at different scan rates in the non-faradaic region (0.04–0.09 V *vs.* RHE) using 0.1 M potassium phosphate solution as the electrolyte with an assumption that double-layer charging is the only process in this potential range. The slopes of the straight-line parts of the capacitive current densities *vs.* scan rates (see ESI, section S2.5†) give the double layer capacitance values 1.3467×10^{-4} F cm^{-2} and 1.9827×10^{-4} F cm^{-2}, respectively for compounds **1** and **2**. In a similar way, the double-layer capacitance of the bare nickel foam (NiFO) electrode is measured and found to be 0.848×10^{-4} F cm^{-2}. Thus, the capacitance values also follow the same trend that compound **2** performs some-what better than compound **1** in the present study. The electrochemically active surface areas (EASAs) of NiFO-blank, compounds **1** and **2** (on nickel foams) are calculated from the double-layer capacitance values (Fig. S15, ESI†) and are found to be 1.388 cm^2, 2.204 cm^2, and 3.245 cm^2 for NiFO-blank, compounds **1** and **2**, respectively. The detailed calculations are provided with ESI (section S2.5†). Subsequently, the EASA values are applied to estimate the specific current densities to obtain the EASA-normalized polarization curves of NiFO-blank, compounds **1** and **2** (Fig. S16, ESI†).

The required overpotential (η) values to drive the HER current density of 10 mA cm^{-2} are found to be −726.04 mV and −643.52 mV for compounds **1** and **2**, respectively (Fig. 8a). Thus, the comparison of values of Tafel slopes and overpotentials of **1** and **2** clearly indicates that compound **2** outperforms compound **1** as far as overall electrocatalytic HER is concerned. The obtained overpotential values are comparable to the values reported for various other relevant systems for the current density of 10 mA cm^{-2}.[28,50–54] Faradaic efficiencies, *i.e.*, the efficiencies of conversion of electrical energy to chemical energy, for both the catalysts were obtained by measuring the amounts of evolved hydrogen gas under chronoamperometric measurements using a homemade setup. The relevant details are given in ESI (section S2.6†). The obtained faradaic efficiencies (FEs) of compounds **1** and **2** are found to be 90.9% and 95.7%, respectively. This supports that no major simultaneous side reactions take place in both catalyses.

The relevant turnover frequency (TOF) values were determined from the galvanostatic Tafel plots. The complete coated material on the working electrode is expected to be catalytically active for HER in the present study, because the crystals of compounds **1** and **2** are porous in nature (referring to their crystal structure analyses, see Fig. S2 and S3 in ESI†). We have also performed their pore volume analyses by gas adsorption studies (see ESI, section S2.7†). We have thus assumed that the internal surface areas of the catalysts can be accessible in the overall catalysis. Therefore, the lower limits of TOF values of catalysts **1** and **2** were calculated by accounting for the total amounts of catalysts present in the respective coated samples and not by the surface coverage of the active species. The obtained (lower limit) TOF values are 0.593 s^{-1} and 0.634 s^{-1} for **1** and **2** respectively indicating a moderate HER catalytic efficiency in the present work (see ESI, section S2.8† for details). Even though we have presumed that the whole coated material on the working electrode may be catalytically active towards HER, it is important to mention that practically only a small fraction is expected to remain exposed. Thus, the surface coverages by catalysts **1** and **2** should be much lower than the total amount of respective catalysts present in the coated material. Therefore, the actual TOF values may be much higher than the reported ones here. Stability experiments (10 hours CA electrolysis and 1000 cycles CVs) along with all the kinetic parameters (such as Tafel slope, EIS, C_{dl}, overpotential, FEs, and TOF values) unambiguously establish that compounds **1** and **2** are poten-

tial HER electrocatalysts and compound **2** outperforms compound **1** in the present work.

Conclusions

In this study, we intended to establish that if W^{VI}–OH functionality is grafted on a polyoxometalate (POM) cluster surface, the resulting POM can be used as an electrocatalyst for HER by water reduction. We have successfully demonstrated this structure–function relationship model by studying two POM-based compounds **1** and **2**, each having two –*cis*{$W^{VI}(OH)_2$} moieties as active sites for HER. The obtained kinetic parameters and stability experiments suggest that both the electrocatalysts (**1** and **2**) are efficient and robust for electrocatalytic HER. In particular, we have successfully designated and generalized the role of a well-defined functional group on a POM surface that can be used for introducing electrocatalytic HER properties to POMs. From this work, we predict that a POM compound, known or unknown, having M–OH group/functionality can be active towards electrochemical HER. This structure–function relation and the observed hierarchical HER trend provide the necessary toolkits for further introduction of more number of active sites (M–OH) and molecular modulation for the next level catalysts to sustainably harvest clean energy. This work will not only have an impact in the area of polyoxometalate chemistry but also in the area of inorganic materials chemistry, in general, in the sense that there are numerous polyoxometalate-based metal–oxide compounds, and any compound among these, having M–OH functionality, would exhibit hydrogen evolution reaction (HER).

Author contributions

The manuscript was written through the contributions of all authors. All authors have given approval to the final version of the manuscript.

Conflicts of interest

The authors declare no competing financial interests.

Acknowledgements

We thank SERB, DST, Government of India (Project No. EMR/2017/002971) for financial support. We acknowledge the UGC-BSR-Mid-Career Award Project (Project No. 19-232/2019 (BSR)). We also acknowledge IoE, University of Hyderabad (Project No. RC1-20-007) for financial support.

References

1 R. Subbaraman, D. Tripkovic, K.-C. Chang, D. Strmcnik, A. P. Paulikas, P. Hirunsit, M. Chan, J. Greeley, V. Stamenkovic and N. M. Markovic, Trends in activity for the water electrolyser reactions on 3d M(Ni, Co, Fe, Mn) hydr(oxy)oxide catalysts, *Nat. Mater.*, 2012, **11**, 550–557.

2 R. Subbaraman, D. Tripkovic, D. Strmcnik, K.-C. Chang, M. Uchimura, A. P. Paulikas, V. Stamenkovic and N. M. Markovic, Enhancing hydrogen evolution activity in water splitting by tailoring Li^+-$Ni(OH)_2$-Pt interfaces, *Science*, 2011, **334**, 1256–1260.

3 L. Zhang and Z. Chen, Polyoxometalates: tailoring metal oxides in molecular dimension toward energy applications, *Int. J. Energy Res.*, 2020, **44**, 3316–3346.

4 I. Roger, M. A. Shipman and M. D. Symes, Earth-abundant catalysts for electrochemical and photoelectrochemical water splitting, *Nat. Rev. Chem.*, 2017, **1**, 0003.

5 J.-J. Chen, M. D. Symes and L. Cronin, Highly reduced and protonated aqueous solutions of $[P_2W_{18}O62]^{6-}$ for on-demand hydrogen generation and energy storage, *Nat. Chem.*, 2018, **10**, 1042–1047.

6 Y. Lei, Y. Wang, Y. Liu, C. Song, Q. Li, D. Wang and Y. Li, Designing atomic active centers for hydrogen evolution electrocatalysts, *Angew. Chem., Int. Ed.*, 2020, **59**, 20794–20812.

7 X. Zou and Y. Zhang, Noble metal-free hydrogen evolution catalysts for water splitting, *Chem. Soc. Rev.*, 2015, **44**, 5148–5180.

8 M. Martin-Sabi, J. Soriano-López, R. S. Winter, J.-J. Chen, L. Vilà-Nadal, D.-L. Long, J. R. Galán-Mascarós and L. Cronin, Redox tuning the Weakley-type polyoxometalate archetype for the oxygen evolution reaction, *Nat. Catal.*, 2018, **1**, 208–213.

9 J. Zhu, L. Hu, P. Zhao, L. Y. S. Lee and K.-Y. Wong, Recent advances in electrocatalytic hydrogen evolution using nanoparticles, *Chem. Rev.*, 2020, **120**, 851–918.

10 J. Park, T. Kwon, J. Kim, H. Jin, H. Y. Kim, B. Kim, S. H. Joo and K. Lee, Hollow nanoparticles as emerging electrocatalysts for renewable energy conversion reactions, *Chem. Soc. Rev.*, 2018, **47**, 8173–8202.

11 G. Chisholm, L. Cronin and M. D. Symes, Decoupled electrolysis using a silicotungstic acid electron-coupled-proton buffer in a proton exchange membrane cell, *Electrochim. Acta*, 2020, **331**, 135255.

12 V. S. Thoi, Y. Sun, J. R. Long and C. J. Chang, Complexes of earth-abundant metals for catalytic electrochemical hydrogen generation under aqueous conditions, *Chem. Soc. Rev.*, 2013, **42**, 2388–2400.

13 B. Nohra, H. E. Moll, L. M. R. Albelo, B. Keita, L. Nadjo, A. Dolbecq, P. Mialane, J. Marrot, C. Mellot-Draznieks, M. O'Keeffe, R. N. Biboum and J. Lemaire, Polyoxometalate-based metal organic frameworks (POMOFs): structural trends, energetics, and high electrocatalytic efficiency for hydrogen evolution reaction, *J. Am. Chem. Soc.*, 2011, **133**, 13363–13374.

14 J. Tourneur, B. Fabre, G. Loget, A. Vacher, C. Mériadec, S. Ababou-Girard, F. Gouttefangeas, L. Joanny, E. Cadot, M. Haouas, N. Leclerc-Laronze, C. Falaise and E. Guillon, Molecular and material engineering of photocathodes deri-

vatized with polyoxometalate-supported $\{Mo_3S_4\}$ HER catalysts, *J. Am. Chem. Soc.*, 2019, **141**, 11954–11962.

15 J. T. Rhule, C. L. Hill, D. A. Judd and R. F. Schinazi, Polyoxometalates in medicine, *Chem. Rev.*, 1998, **98**, 327–358.

16 A. Müller, F. Peters, M. T. Pope and D. Gatteschi, Polyoxometalates: very large clusters nanoscale magnets, *Chem. Rev.*, 1998, **98**, 239–272.

17 M. Ibrahim, Y. Xiang, B. S. Bassil, Y. Lan, A. K. Powell, P. de Oliveira, B. Keita and U. Kortz, Synthesis, magnetism, and electrochemistry of the Ni_{14}- and Ni_5-containing heteropolytungstates $[Ni_{14}(OH)_6(H_2O)_{10}(HPO_4)_4(P_2W_{15}O_{56})4]^{34-}$ and $[Ni_5(OH)_4(H_2O)_4(\beta\text{-}GeW_9O_{34})(\beta\text{-}GeW_8O_{30}(OH))]^{13-}$, *Inorg. Chem.*, 2013, **52**, 8399–8408.

18 M. Sadakane and E. Steckhan, Electrochemical properties of polyoxometalates as electrocatalysts, *Chem. Rev.*, 1998, **98**, 219–238.

19 H. N. Miras, J. Yan, D.-L. Long and L. Cronin, Engineering polyoxometalates with emergent properties, *Chem. Soc. Rev.*, 2012, **41**, 7403–7430.

20 H. K. Kolli, D. Jana and S. K. Das, Nanoblackberries of $\{W_{72}Fe33\}$ and {Mo72Fe30}: electrocatalytic water reduction, *Inorg. Chem.*, 2021, **60**, 15569–11558.

21 D. M. Fernandes, M. P. Araújo, A. Haider, A. S. Mougharbel, A. J. S. Fernandes, U. Kortz and C. Freire, Polyoxometalate–graphene electrocatalysts for the hydrogen evolution reaction, *ChemElectroChem*, 2018, **5**, 273–283.

22 H. Lv, Y. V. Geletii, C. Zhao, J. W. Vickers, G. Zhu, Z. Luo, J. Song, T. Lian, D. G. Musaevb and C. L. Hill, Polyoxometalate water oxidation catalysts and the production of green fuel, *Chem. Soc. Rev.*, 2012, **41**, 7572–7589.

23 N. Li, J. Liu, B.-X. Dong and Y.-Q. Lan, Polyoxometalate–based compounds for photo– and electrocatalytic applications, *Angew. Chem., Int. Ed.*, 2020, **59**, 20779–20793.

24 J. Li, C. A. Triana, W. Wan, D. P. A. Saseendran, Y. Zhao, S. E. Balaghi, S. Heidari and G. R. Patzke, Molecular and heterogeneous water oxidation catalysts: recent progress and joint perspectives, *Chem. Soc. Rev.*, 2021, **50**, 2444–2485.

25 F. Evangelisti, P.-E. Car, O. Blacque and G. R. Patzke, Photocatalytic water oxidation with cobalt-containing tungstobismutates: tuning the metal core, *Catal. Sci. Technol.*, 2013, **3**, 3117–3129.

26 T. Ueda, Electrochemistry of polyoxometalates: from fundamental aspects to applications, *ChemElectroChem*, 2018, **5**, 823–838.

27 M. R. Horn, A. Singh, S. Alomari, S. Goberna-Ferrón, R. Benages-Vilau, N. Chodankar, N. Motta, K. Ostrikov, J. MacLeod, P. Sonar, P. Gomez-Romero and D. Duba, Polyoxometalates (POMs): from electroactive clusters to energy materials, *Energy Environ. Sci.*, 2021, **14**, 1652–1700.

28 Y.-X. Ding, Q.-H. Zheng, M.-T. Peng, C. Chen, K.-F. Zou, B.-X. Dong, W.-L. Liu and Y.-L. Teng, A new ε-Keggin polyoxometalate-based metal-organic framework: from design and synthesis to electrochemical hydrogen evolution, *Catal. Commun.*, 2021, **161**, 106367.

29 J.-S. Li, Y.-J. Tang, C.-H. Liu, S.-L. Li, R.-H. Li, L.-Z. Dong, Z.-H. Dai, J.-C. Baoa and Y.-Q. Lan, Polyoxometalate-based metal–organic framework-derived hybrid electrocatalysts for highly efficient hydrogen evolution reaction, *J. Mater. Chem. A*, 2016, **4**, 1202–1207.

30 C. Singh, A. Haldar, O. Basu and S. K. Das, Devising a polyoxometalate-based functional material as an efficient electrocatalyst for the hydrogen evolution reaction, *Inorg. Chem.*, 2021, **14**, 10302–10314.

31 I. Loose, E. Droste, M. Bösing, H. Pohlmann, M. H. Dickman, C. Rosu, M. T. Pope and B. Krebs, Heteropolymetalate clusters of the subvalent main group elements Bi^{III} and Sb^{III}, *Inorg. Chem.*, 1999, **38**, 2688–2694.

32 L. Wang, K. Yu, J. Zhu, B.-B. Zhou, J. R. Liu and G. Y. Yang, Inhibitory effects of different substituted transition metal-based krebs-type sandwich structures on human hepatocellular carcinoma cells, *Dalton Trans.*, 2017, **46**, 2874–2883.

33 L. Wang, B.-B. Zhou, K. Yu, Z.-H. Su, S. Gao, L.-L. Chu, J.-R. Liu and G.-Y. Yang, Novel antitumor agent, trilacunary keggin-type tungstobismuthate, inhibits proliferation and induces apoptosis in human gastric cancer SGC-7901 cells, *Inorg. Chem.*, 2013, **52**, 5119–5127.

34 L. Wang, K. Yu, B.-B. Zhou, Z.-H. Su, S. Gao, L.-L. Chu and J.-R. Liu, The inhibitory effects of a new cobalt-based polyoxometalate on the growth of human cancer cells, *Dalton Trans.*, 2014, **43**, 6070–6078.

35 M. Bösing, I. Loose, H. Pohlmann and B. Krebs, New strategies for the generation of large heteropolymetalate clusters: the β–B–SbW_9 fragment as a multifunctional unit, *Chem. – Eur. J.*, 1997, **3**, 1232–1237.

36 L.-H. Bi and U. Kortz, Synthesis and structure of the pentacopper(II) substituted tungstosilicate $[Cu_5(OH)_4(H_2O)_2(A\text{-}\alpha\text{-}SiW_9O_{33})_2]^{10-}$, *Inorg. Chem.*, 2004, **43**, 7961–7962.

37 S. Nellutla, J. Van Tol, N. S. Dalal, L.-H. Bi, U. Kortz, B. Keita, L. Nadjo, G. A. Khitrov and A. G. Marshall, Magnetism, Electron paramagnetic resonance, electrochemistry, and mass spectrometry of the pentacopper(II)-substituted tungstosilicate $[Cu_5(OH)_4(H_2O)_2(A\text{-}\alpha\text{-}SiW_9O_{33})_2]^{10-}$, a model five-spin frustrated cluster, *Inorg. Chem.*, 2005, **44**, 9795–9806.

38 H. Lv, Y. Chi, J. Leusen, P. Kçgerler, Z. Chen, J. Bacsa, Y. V. Geletii, W. Guo, T. Lian and C. L. Hill, $[\{Ni_4(OH)_3AsO_4\}_4(B\text{–}\alpha\text{–}PW_9O_{34})_4]^{28-}$: A new polyoxometalate structural family with catalytic hydrogen evolution activity, *Chem. – Eur. J.*, 2015, **21**, 17363–17370.

39 S.-X. Guo, C.-Y. Lee, J. Zhang, A. M. Bond, Y. V. Geletii and C. L. Hill, Mediator enhanced water oxidation using $Rb_4[Ru^{II}(bpy)_3]_5[\{Ru^{III}{}_4O_4(OH)_2(H_2O)_4\}(\gamma\text{-}SiW_{10}O36)2]$ Film modified electrodes, *Inorg. Chem.*, 2014, **53**, 7561–7570.

40 M. Bösing, A. Nöh, I. Loose and B. Krebs, Highly efficient catalysts in directed oxygen-transfer processes: synthesis, structures of novel manganese-containing heteropolyanions, and applications in regioselective epoxidation of dienes with hydrogen peroxide, *J. Am. Chem. Soc.*, 1998, **120**, 7252–7259.

41 D. Fang, F. He, J. Xie and L. Xue, Calibration of binding energy positions with C1s for XPS results, *J. Wuhan Univ. Technol., Mater. Sci. Ed.*, 2020, **35**, 711–718.
42 T. L. Barr, An ESCA study of the termination of the passivation of elemental metals, *J. Phys. Chem.*, 1978, **82**, 1801–1810.
43 N. Y. Topsoe, J. A. Dumesic and H. Topsoe, Vanadia-Titania Catalysts for selective catalytic reduction of nitric-oxide by ammonia: I.I. studies of active sites and formulation of catalytic cycles, *J. Catal.*, 1995, **151**, 241–252.
44 N. Y. Topsoe, H. Topsoe and J. A. Dumesic, Vanadia/Titania catalysts for selective catalytic reduction (SCR) of nitric-oxide by ammonia: I. combined temperature-programmed in-situ ftir and on-line mass-spectroscopy studies, *J. Catal.*, 1995, **151**, 226–240.
45 J. N. Hausmann, S. Mebs, K. Laun, I. Zebger, H. Dau, P. W. Menezes and M. Driess, Understanding the formation of bulk- and surface-active layered (oxy)hydroxides for water oxidation starting from a cobalt selenite precursor, *Energy Environ. Sci.*, 2020, **13**, 3607–3619.
46 S. Anantharaj, S. Noda, V. R. Jothi, S. C. Yi, M. Driess and P. W. Menezes, Strategies and perspectives to catch the missing pieces in energy–efficient hydrogen evolution reaction in alkaline media, *Angew. Chem., Int. Ed.*, 2021, **60**, 2–28.
47 J.-C. Liu, B. Qi and Y.-F. Song, Engineering polyoxometalate-intercalated layered double hydroxides for catalytic applications, *Dalton Trans.*, 2020, **49**, 3934–3941.
48 T. Shinagawa, A. T. Garcia-Esparza and K. Takanabe, Insight on tafel slopes from a microkinetic analysis of aqueous electrocatalysis for energy conversion, *Sci. Rep.*, 2015, **5**, 13801.
49 T. Shinagawa and K. Takanabe, Towards versatile and sustainable hydrogen production through electrocatalytic water splitting: electrolyte engineering, *ChemSusChem*, 2017, **10**, 1318–1336.
50 M. H. Tran, T. Schafer, A. Shahraei, M. Durrschnabel, L. Molina-Luna, U. I. Kramm and C. S. Birkel, Adding a new member to the MXene family: synthesis, structure, and electrocatalytic activity for the hydrogen evolution reaction of $V_4C_3T_x$, *ACS Appl. Energy Mater.*, 2018, **1**, 3908–3914.
51 Z. W. Seh, K. D. Fredrickson, B. Anasori, J. Kibsgaard, A. L. Strickler, M. R. Lukatskaya, Y. Gogotsi, T. F. Jaramillo and A. Vojvodic, Two-dimensional molybdenum carbide (MXene) as an efficient electrocatalyst for hydrogen evolution, *ACS Energy Lett.*, 2016, **1**, 589–594.
52 M. Zubair, M. M. U. Hassan, M. T. Mehran, M. M. Bai, S. Hussain and F. Shahzad, 2D MXenes and their heterostructures for HER, OER and overall water splitting: a review, *Int. J. Hydrogen Energy*, 2022, **47**, 2794–2818.
53 H. Peng, X. Yang, Y. Ma, J. Liu, Y. Wang, H. Tan and Y. Li, Polyoxometalate-based metal–organic framework loaded with an ultralow amount of Pt as an efficient electrocatalyst for hydrogen production, *CrystEngComm*, 2018, **20**, 5387–5394.
54 J.-S. Qin, D.-Y. Du, W. Guan, X.-J. Bo, Y. Li, L. Guo, Z.-M. Su, Y.-Y. Wang, Y.-Q. Lan and H.-C. Zhou, Ultrastable polymolybdate-based metal-organic frameworks as highly active electrocatalysts for hydrogen generation from water, *J. Am. Chem. Soc.*, 2015, **137**, 7169–7177.